High-gain circularly polarized metasurface antenna for NR257 band millimeter-wave 5G communication

Praveen Haandi Lakshman[1], Yerriswamy Thatti[2], Puneeth Kumar Tharehalli Rajanna[3], Shambulinga Mudukavvanavar[4]

[1]Department of Electronics and Communication Engineering, Shri Dharmasthala Manjunatheshwara Institute of Technology, Ujire, India
[2]Department of Computer Science Engineering, KLEIT, Hubballi, India
[3]Department of Electronics and Telecommunication Engineering, Siddaganga Institute of Technology, Tumkur, India
[4]Department of Electronics and Telecommunication Engineering, RVCE, Bengalauru, India

Article Info

ABSTRACT

A metasurface inspired circularly polarized (CP) compact patch antenna with high gain for fifth-generation communication systems is designed and implemented in this article. The proposed structure features a corner truncated patch antenna and a metasurface of 3×3 double sided identical circular metallic patches. The attribute that puts this design distinct is that it minimizes the impact of scattering and edge diffraction at millimeter wave frequencies. The metasurface above a patch with an air gap is designed using the similar substrate material with the same thickness, resulting in a simplified antenna design with high gain and low cost. The antenna's overall dimension is $1.1\lambda_0$ x $1.1\lambda_0$ x $0.2\lambda_0$, with a peak gain of 11.5 dBic and a 3-dB axial ratio bandwidth of 28.45 - 28.88 GHz. The simulated and experimental results show that the metasurface-inspired antenna has better impedance matching and radiation efficiency between 28.23-30.01 GHz. Additionally, the experimental results of the proposed antenna exhibits stable right-hand circular polarization in the desired frequency range and a flat gain response with a little variation. The proposed antenna design could be well suited for millimeter-wave communication systems, in scenarios requiring robust long-range performance and high data throughput.

Corresponding Author:

Praveen Haandi Lakshman
Department of Electronics and Communication Engineering, SDM Institute of Technology
Ujire, Karnataka, India-574240
Email: praveee79@gmail.com

1. INTRODUCTION

The significant increase in annual data traffic is projected to require higher capacity, improved reliability, greater velocity, reduced latency, and extensive connectivity. Fifth-generation wireless communication network is the essential answer to address the aforementioned difficulties and facilitate potential applications [1]-[3]. 5G communication technology uses two standardized frequency bands: one band operates below 6 GHz, known as the sub-6 GHz band, while the other is the millimeter wave band. The n257 band, often known as 28 GHz, is being standardized by the majority of countries for their 5G communications [4]. High-gain antennas help mm-wave communication systems overcome challenges posed by atmospheric attenuation and propagation losses, which can negatively impact signal strength [5]-[7].

Antennas with circular polarization (CP) are favoured owing to their increased immunity to interference, losses caused by misalignment, multi-path fading, and Faraday's rotation [8]. Microstrip patches

are employed in the construction of CP antennas because of their advantageous characteristics, including their structure, cost-effectiveness, and ease of integration [9]. Obtaining high gain and CP is challenging when using conventional microstrip antennas. The enhancement of antenna gain for millimeter-wave systems is needed to improve the communication over long distance. This has led researchers to employ a variety of strategies, including stacking approaches, array formation, superstrate technique, substrate-integrated waveguide (SIW) approaches, and many more. Metasurface technique is used in this study to enhance the gain, so that path losses can be reduced in mm waves, which enables higher data rates and offers low latency. Its compact design, higher precision control, and improved integration over other traditional methods are its main advantages. Two-dimensional metasurfaces/metamaterials, offer a convenient and uncomplicated method for producing high-gain millimeter-wave antennas for 5G applications [10], [11]. By utilising single-layer or multi-layer stacks of planar structures, it is feasible to attain a broad axial ratio bandwidth and improve the antenna's gain without compromising its low profile [12], [13]. An air gap is strategically placed either above [14], [15] or below [16], [17] the primary source in order to accommodate the metasurface.

Only a few numbers of metasurface antennas with linear polarization have been developed for millimeter wave frequencies. When designing antennas for mm-Wave frequencies, a variety of techniques can be employed to enhance gain. To enhance patch antenna gain and bandwidth and reduce its radar cross section, a reflective frequency selective surface superstrate is positioned above it [18]. Radial-phase gradient metalens with a single layer offer greater gain, but their effectiveness is restricted due to their limited range of frequencies [19]. The bowtie antenna is enhanced for beam splitting and gain by integrating a metamaterial array with a high refractive index [20]. The utilization of multiple input multiple output (MIMO) antennas using a metasurface array based on a single-layered circular split-ring resonator [21], slotted patch antennas, and MIMO setups employing split-ring resonator based metasurface [22], [23] has demonstrated efficiency in enhancing the gain. However, these approaches suffer from low radiation efficiency and a high antenna profile. The above mentioned techniques provide a comprehensive study of gain enhancement in both single and multi-layered mediums, but their applicability is restricted to linear polarization (LP) scenarios.

The gain is enhanced by employing a uniform partially reflecting surface (PRS) superstrate [24] and PRS as a uniform dielectric slab on top of the radiator [25]. A wideband CP corner truncated and diagonally slotted patch with a square ring metamaterial structure described in [26] and a square metallic patch metasurface described in [27] have been developed with MIMO configuration. End-fire dipole arrays are placed below CP antennas with non-uniform circular patches and crossslot metasurfaces. This configuration results in significant gain and wideband performance. However, it should be noted that the construction of the dipoles is complex [28]. A square patch-based metasurface with a truncated corner and a two-layer SIW feed structure is proposed to provide a wide CP bandwidth [29]. The CP-based antennas discussed above, which are intended for millimeter wave bands, suffer from drawbacks such as complicated fabrication processes, a more number of unit cells in metasurface, and an increased antenna profile.

The proposed design, utilizes a metasurface-based approach to achieve high gain for the 28 GHz millimeter wave frequency range. The suggested design is unique because it presents a challenge in achieving high gain and CP at millimeter wave frequency, while maintaining compact size. A square patch antenna produces two degenerate modes by truncating its corners, which is necessary to achieve circular polarization. A single-patch antenna can achieve a gain of 6 dBiC. In order to enhance the signal reception over the CP antenna, a circular shaped unit cell based metasurface layer is mounted. When compared to alternative patch designs such as square, triangular, and rectangular, a circular-shaped unit cell offers the benefit of minimizing the impact of losses such as scattering and edge diffraction at millimeter-wave frequencies. The metasurface recommended has improved the radiation efficiency at 28.6 GHz to above 80%, resulting in a total gain of the antenna of 11.5 dBiC. The proposed design is characterised by its compact size and features such as CP and high gain, making it highly suitable for millimeter-wave wireless applications. Finally, the paper is organised as: i) introduction, ii) proposed antenna design, analysis, and operation principle are detailed, along with unit cell characterization, iii) results and discussion, and iv) conclusion.

2.   ANTENNA GEOMETRY AND DESIGN PRINCIPLE

Figure 1 presents structure of the proposed antenna with metasurface where Figure 1(a) shows the top view of the proposed antenna and Figure 1(b) depict a square patch corner truncated antenna fed by a quarter wave transformer and Figure 1(c) shows the side view of the proposed antenna. The Rogers Duroid 5880 substrate is used to fabricate patch antennas with identical properties, such as $\epsilon_r = 2.2$, $\tan\delta = 0.0009$, and h_s=0.252 mm. The structure of metasurface consists of a periodic array of symmetrical double-sided identical circular metallic patches arranged in a 3×3 grid. The adjacent unit cell distance is represented

by 'g'. The metasurface layer is positioned over the patch with a 1.72 mm distance of air between them. The antenna has a total size of $12\times12\times 2.26\ mm^3$, which is equivalent to $1.1\lambda_0\times1.1\lambda_0\times0.2\lambda_0$, times the free-space wavelength of 28.6 GHz. Prior to fabrication, the following parameters must be optimized in order for the antenna to function efficiently at its optimised dimensions: 'A' is equal to 12. The value of W_p is equal to 3.33. The values of W_{f1} and L_{f1} are 0.741 and 2.02 respectively. The values of W_f and L_f are 0.7826 and 1.9581 respectively. The value of 'a' is 0.64918, R_1 is equal to 1.9. The value of 'g' is 0.1. The value of h_m is 1.762 (unit=mm). CST microwave studio is used for the purpose of simulating design and analysis.
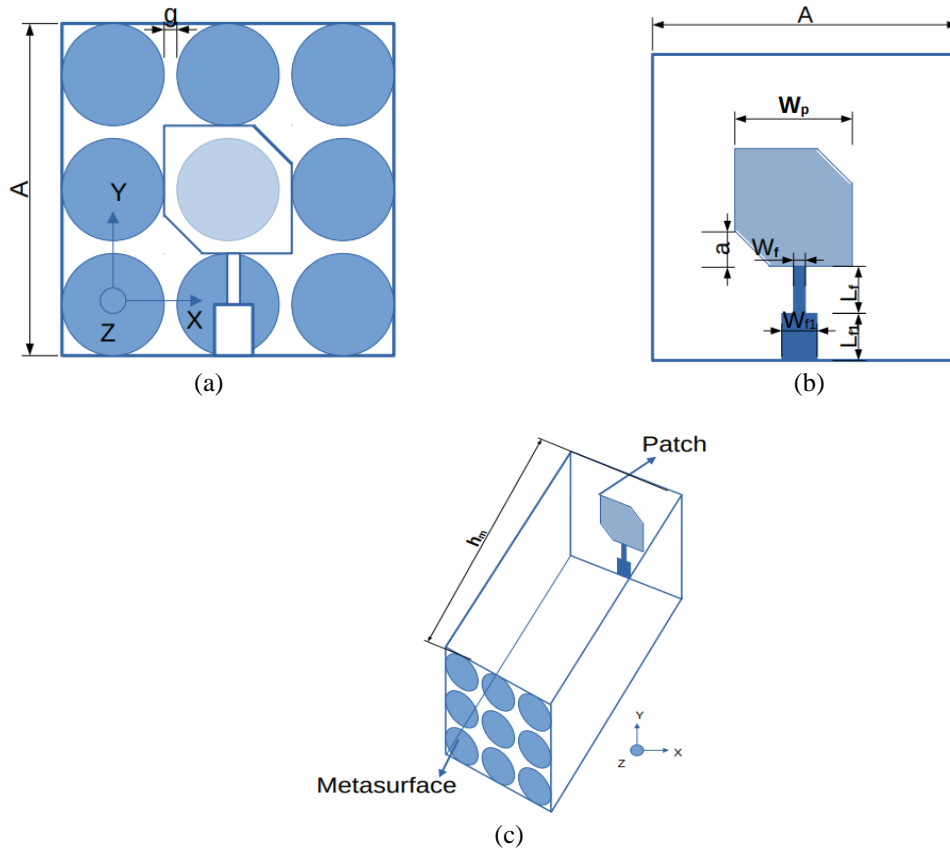

Figure 1. Proposed antenna with metasurface: (a) top view, (b) corner truncated patch antenna, and (c) side view

2.1. Antenna design procedure

The proposed structure of the corner truncated square microstrip patch antenna as shown in the Figure 1(b) is designed to work at millimetre-wave frequencies, because of its low dielectric and dispersion loss, Rogers Duroid 5880 substrate material is selected and it is highly efficient at higher frequencies than most other substrates [30]. Firstly, the dimensional area for the square patch is calculated through the use of transmission line model. The parameters of antenna design are calculated by using the (1) [31].

$$f_r = \frac{c}{2*W_p} \sqrt{\frac{2}{1+\epsilon_r}} \tag{1}$$

The symbol 'W_p'' denotes patch width, 'f_r' represents the resonance frequency, 'c' stands for the velocity of light, and 'ϵ_r'' signifies the relative permittivity. The quarter-wave transformer is commonly used for impedance matching. The relationship between the load impedance 'Z_L'', input impedance 'Z_{in}'', and the characteristic impedance 'Z_0'' of 50 ohms is described by equations [32], [33]. LP radiation is produced by square patch antenna by using (2).

$$Z_0 = \sqrt{Z_{in} * Z_L} \tag{2}$$

One approach employed to generate CP radiation is the truncation of corners [34]. The unloaded quality factor of the patch, 'Q_0', is initially determined using the cavity model. This factor is typically influenced by the dielectric constant 'ε_r' and the substrate thickness 'h_s' by (3):

$$Q_0 = \frac{c\sqrt{\varepsilon_r}}{4f_r h_s} \qquad (3)$$

from this equation the truncation ratio '$\frac{\Delta s}{s}$' is known i.e by using the (4):

$$\frac{\Delta s}{s} = \frac{1}{2Q_0} \qquad (4)$$

the length of truncation 'a' for the patch is calculated by using equation, where 'L' is the actual length of the patch by (5).

$$a = L\sqrt{\frac{\Delta s}{s}} \qquad (5)$$

By reducing the corner diagonals with optimised sides of the same length, the primary mode becomes two perpendicular modes with similar strengths, which in turn result in circular polarization. In order to gain a deeper understanding of achieving circular polarization, Figure 2 shows the surface current distribution of patch antenna examined at different instances of time at 28.6 GHz. In the upward direction (+ z-direction), Figure 2(a) and Figure 2(b) exhibit surface current at ωt = 0° and ωt = 90°, with Figure 2(c) and Figure 2 (d) exhibit surface current at ωt = 180° and ωt = 270°. The RHCP radiation is generated by the surface current that rotates anticlockwise at a frequency of 28.6 GHz.
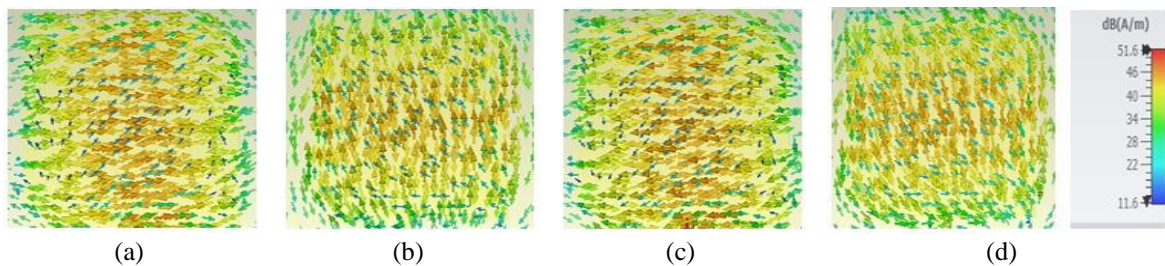

Figure 2. Surface current distribution of patch antenna at different instances: (a) ωt = 0°, (b) ωt = 90°,
(c) ωt = 180°, and (d) ωt = 270°

2.2. Metasurface unit cell

Figure 3 depicts the proposed metsurface unit cell, in which Figure 3(a) shows the simulation setup, which includes the boundary conditions, and the design for the metasurface unit cell. Set of unit cell array referred as metasurface is fabricated using Rogers Duroid 5880 substrate, which has a thickness of h_s = 0.252 mm and a tanδ value of 0.0009. A circular metallic patch that is symmetrical is etched onto the substrate's top and bottom surfaces. The unit cell has the following dimensions: the width 'W' and length 'L' are both 4 mm, the radius 'R_1' is 1.9 mm, and the thickness 't' is 0.017 mm. Along the z-axis, two wave guiding ports are on opposite sides of the unit cell, while periodic boundary conditions are applied in the remaining directions. Figure 3(b) shows the simulated magnitude characteristics of S_{11} and S_{21} for a single unit cell. The unit cell resonates at 28.6 GHz for both x and y-polarization. At this frequency, the transmission coefficient magnitudes are the same. The simulated single-unit cell is constructed by arranging a 3×3 array of metasurfaces. The metasurface demonstrates excellent transmission and reflection coefficients at 28.6 GHz, with a return loss exceeding -25 dB. In order to enhance the gain, the unit cell could be designed as a transmitting surface for primary sources. Figure 3(c) displays the equivalent circuit design, depicting an LC circuit consisting of capacitance and inductance. Through this circuit, the circular patch unit cell's fundamental characteristics are determined.
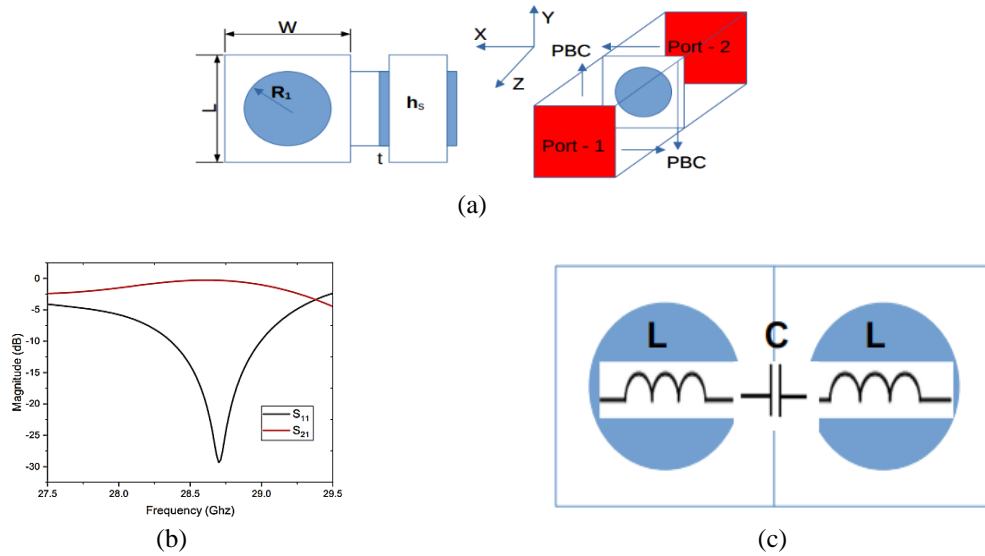
(a)

(b)   (c)

Figure 3. Metasurface unit cell: (a) unit cell and its boundary condition, (b) reflection (S_{11}) and transmission (S_{21}) characteristics, and (c) unit cell with its LC components

The incorporation of periodic structures as metasurface enhances the performance, particularly in terms of operating bandwidth and gain, of CP patch antennas. The metasurface of finite size facilitates the generation of additional resonances through the propagation of surface waves. Effective utilization of these additional resonances results in an increase in gain. Thorough investigation of this approach has already been conducted in references [35]-[37]. Simple prediction of the current central frequency is possible by (6) and (7):

$$\beta_{sw} = \frac{m\pi}{L_{MTS}} \tag{6}$$

$$L_{MTS} = P \times N(x,y) \tag{7}$$

here, the propagation constant of the surface wave at resonance frequency is denoted as 'β_{sw}', the length of the metasurface array is specified as 'L_{MTS}', the periodicity is denoted as P = 4 mm, and the number of unit cells in the x- and y-direction is denoted as N = 3 and m = 1 is considered [36]. Propagation constants of transverse electric (TE) and transverse magnetic (TM) waves is calculated by using the (8) and (9).

$$\beta_{TE} = \frac{\omega}{c}\sqrt{1 - \frac{(Z_{MTS})^2}{(Z_o)^2}} \tag{8}$$

$$\beta_{TM} = \frac{\omega}{c}\sqrt{1 - \frac{(Z_o)^2}{(Z_{MTS})^2}} \tag{9}$$

Let 'ω' represents angular frequency, 'c' denote the speed of light, and 'Z_{MTS}' indicate the surface impedance of the metasurface, while Z_0 represent the impedance in free space. It is anticipated that the TE and TM surface waves will resonate at approximately 28.6 GHz when the metasurface is arranged with N(x,y)=3×3 unit cells. Since the patch resonance is likely to be supported by slow-wave propagation, surface waves are likely to excite. The equivalent circuit diagram, represented as a resonant LC circuit composed of capacitance and inductance, can also be used to anticipate the frequency characteristics of the circular patch metasurface, as shown in Figure 3. The metasurface acts as LC resonant circuit, the inductive part is provided by circular shaped metallic patch and capacitance is obtained by two sided circular metallic patches saperated by dielectric. The circular shaped double sided based metasurface's normalized capacitive susceptance 'B' and inductive reactance 'X' is expressed as (10) and (11):

$$X = \frac{X_L}{Z_0} = \omega\frac{L_{MTS}}{Z_0} \tag{10}$$

$$B = \frac{B_C}{Y_0} = \omega\frac{C_{MTS}\varepsilon_{eff}}{Y_0} \tag{11}$$

Here, 'ω' stands for angular frequency, Z_0 is the free space impedance "i.e." $'Z_0 = 1/Y_0'$, and $'L_{MTS}'$ and $'C_{MTS}'$ stand for the respective inductance and capacitance of the metasurface. The effective permittivity is $'\varepsilon_{eff}'$, while the inductive reactance and capacitive susceptance are $'X_L'$ and $'B_C'$, respectively [38] provides a thorough explanation of the equivalent circuit model used for such metasurface.

2.3. Effect of metasurface

The single-feed patch antenna exhibits less than -10dB impedance (S_{11}) bandwidth, gain, and directivity. A truncated patch antenna is augmented with an metasurface, which is a periodic lattice of double-sided identical circular metallic patches, to improve antenna's performance. The metasurface functions as an auxiliary emitter of radiation, hence enhancing the gain. Figure 4 displays the effect of with and without metasurface, where Figure 4(a) shows the effect on magnitude of reflection coefficient and Figure 4(b) shows the effect of gain of the patch antenna that has been truncated in its corner.

As anticipated, the proposed antenna without metasurface results in a limited antenna gain when compared to the presence of metasurface. Additionally, the magnitude increases from -19 dB to -50 dB. The addition of a metasurface to a patch antenna truncated at its corner results in an improvement in gain from 6 dBiC to 11.5 dBiC. The increased aperture efficiency of the metasurface, in conjunction with the patch antenna, leads to a significant gain enhancement. Consequently, a metasurface with a single layer and double-sided configuration exhibits CP characteristics with enhanced gain. The entire process of designing the metasurface inspired antenna is depicted in Figure 5.
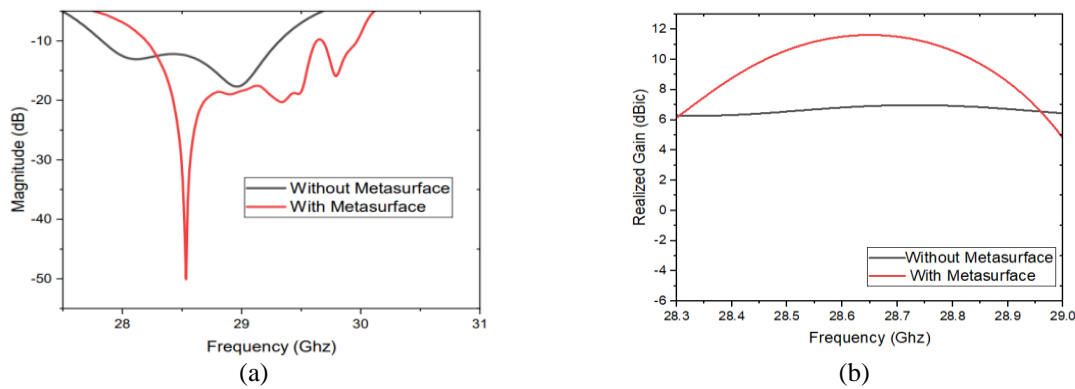

Figure 4. Proposed design with and without metasurface (a) reflection coefficient (S_{11}) and (b) gain
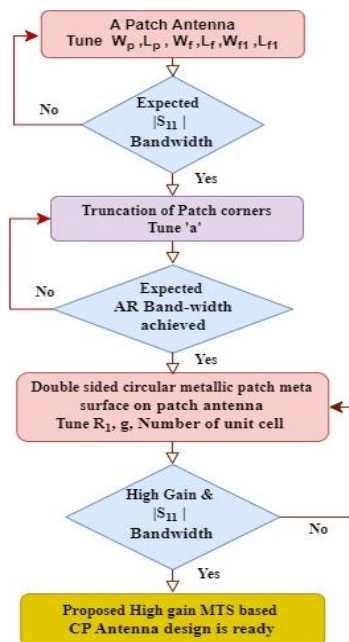

Figure 5. Flowchart of the proposed design

The patch antenna with CP can attain its highest gain in the broadside direction when the height of the cavity matches specific criteria [39] by using the (12):

$$h_m = \frac{\phi_S + \phi_G - 2N\pi}{4\pi} \lambda_0 \quad \text{where} \quad N = 0,1,2 \tag{12}$$

where 'λ_0' is free space wavelength and ϕ_S and ϕ_G are the reflection phase of metasurface and ground plane of the patch antenna, respectively. The value of $h_m = 1.54$ mm is obtained from the (12). Then a parametric inspection has been done to optimize the metasurface layer height (h_m) above the patch antenna to maximize the gain.

Figure 6. displays the parametric analysis of height between patch and metasurface where Figure 6(a) depicts the resonance frequencies, Figure 6(b) shows gain and Figure 6(c) plot the axial ratio effect for various height (h_m) values. The curves show that, when the height has a different value, the gain and the axial ratio values are greatly affected. For the optimized height of $h_m = 1.762$ mm, the maximum gain is within the axial ratio bandwidth.
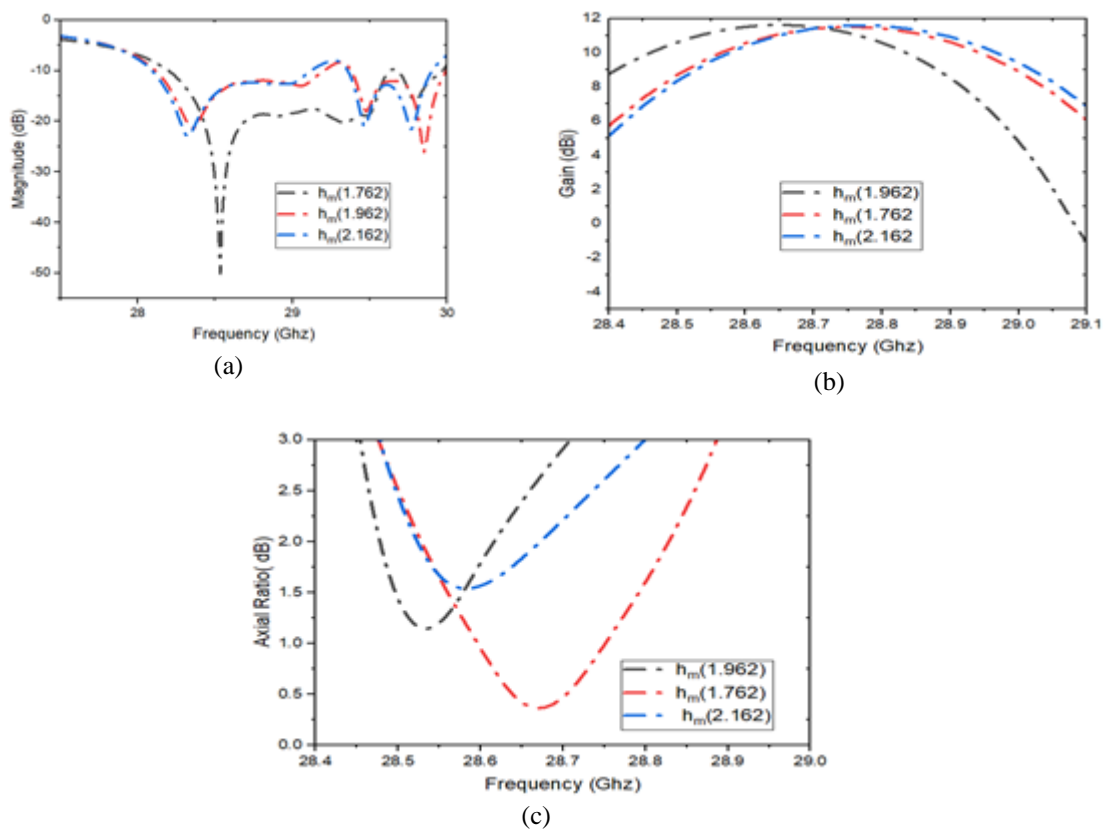

(a)

(b)

(c)

Figure 6. Parametric analysis of height between patch and metasurface (h_m): (a) S_{11}, (b) gain, and
(c) axial ratio

3. RESULTS AND DISCUSSION

A photolithographic fabrication method is used to validate the design concept of the proposed metasurface-based double sided single layered CP antenna prototype. Figure 7(a) shows the fabricated patch antenna, Figure 7(b) shows the fabricated metasurface and Figure 7(c) shows the patch antenna integarated with metasurface. All the photographs of the constructed antenna are displayed in Figure 7. A 50-Ω K-connector with a 2.92mm size is meticulously attached to the patch, and a mechanism of support which enables proper cavity gap between the metasurface and patch is established employing thin plastic rods. An anechoic chamber is used for far-field measurements. The proposed antenna is tested as the receiving antenna (RX), and the transmitting antenna (TX) is a standard gain horn antenna (SGH-series) properly calibrated. Stable power reception was provided by amplifiers; the test antenna was rotated to evaluate the radiation intensity at different orientations. In general, a strong correlation has been established between the observed

and simulated results. The individual parameteric contributions from the fabricated antenna design can be studied by analyzing the results in Figures 8-10. The parameter S_{11} is measured using two port agilent vector network anlayzer.

(a)   (b)   (c)
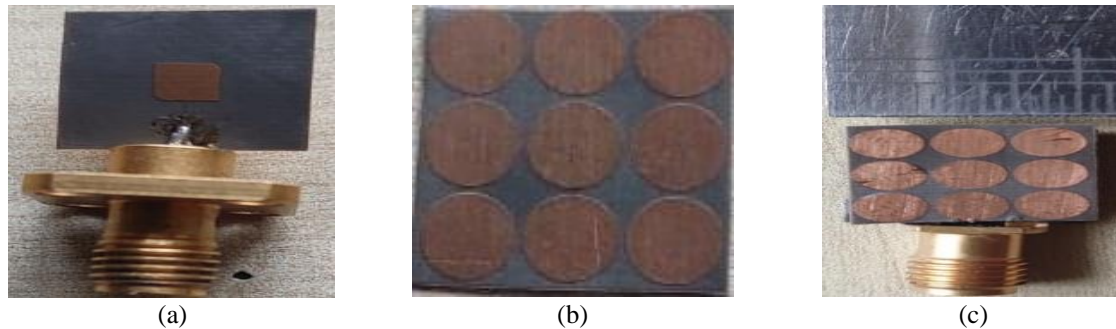
Figure 7. Fabricated model of the proposed design: (a) patch antenna, (b) metasurface (MTS), and (c) high gain CP antenna

Figure 8 shows the antennas measured and simulated S-parameters $|S_{11}|$. The $|S_{11}|$ parameter monitoring is performed using a Rohde and Schwarz ZVA 40 network analyzer, and the measurements are taken in an open air environment. The antenna has a fractional bandwidth of 6.14% relative to the central frequency. It also has sufficient impedance matching, with a $|S_{11}|$ value below -10dB, spanning the frequency range of 28.23-30.01 GHz.

The Figure 9 shows the antenna's radiation properties, specifically the axial ratio and broadside gain. The impedance bandwidth and the obtained 1.39%, 3-dB AR bandwidth, which spans 28.45 to 28.88 GHz, are within the specified impedance bandwidth. Due to difficulties in fabrication, substrate losses and misalignment of the patch on the metasurface layer, simulations and measurements results differed slightly. Furthermore, the antenna achieves a wide gain range of 9.5–11.5 dBic when operating within the frequency range of 28.45–28.88 GHz.
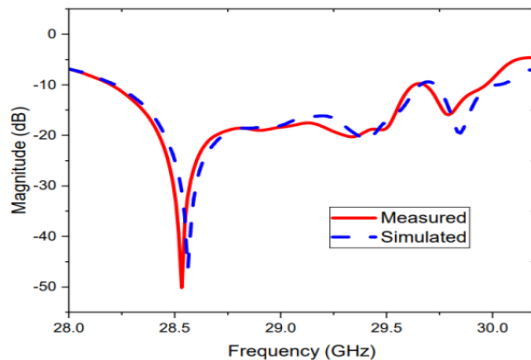

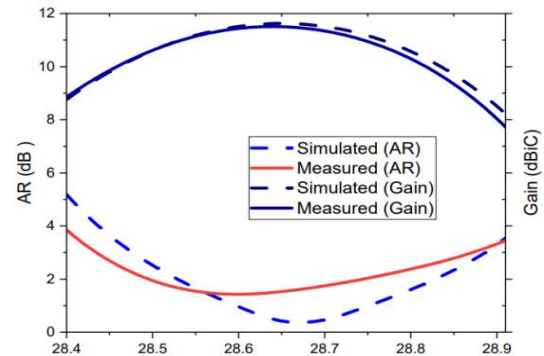Figure 8. The S_{11} experimental results in comparison with simulated results

Figure 9. Axial ratio and gain experimental results in comparison with simulated results

Figure 10 depicts the radiation patterns at a frequency of 28.6 GHz in the two primary planes, where Figure 10(a) shows the xz plane and Figure 10(b) shows yz plane respectively. The radiation patterns of the antenna, which are right-hand circularly polarized (RHCP), are reliable and symmetrical. Throughout the operational frequency range, the left-hand circularly polarised (LHCP) radiation is smaller than the right-hand circularly polarized (RHCP) radiation. The cross-polarization (LHCP) level of more than -20 dB is achieved with respect to co-polarization (RHCP) level at the broadside direction (θ = 0°). The directivity can be determined by using a 3dB beam-width. Theoretically, an aperture antenna's maximum directivity can be computed as $D = 10log(4\pi A/\lambda_0^2) = 11.9$ dB, where $\lambda_0 = c/f$ and $A = 12\ mm \times 12\ mm$. The theoretical directivity matches the physical achievable value of the same-sized proposed antenna.
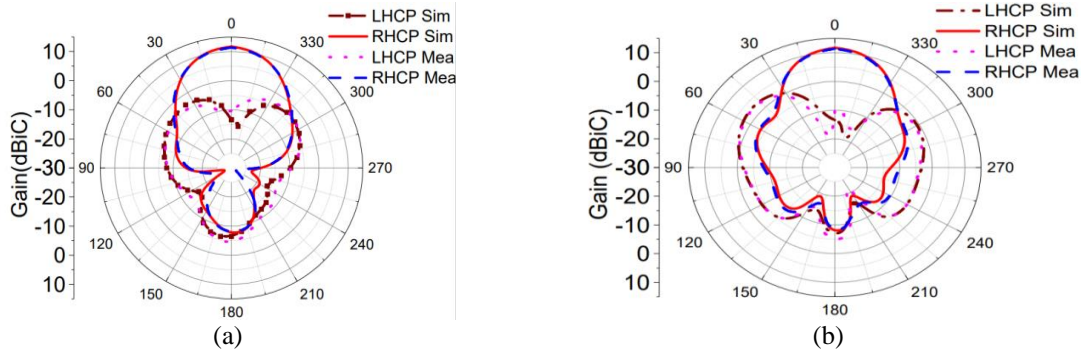
Figure 10. Radiation patterns which were measured and simulated at 28.6 GHz (a) XZ plane and
(b) YZ plane

3.1. Comparision with state-of-the-art-works

Table 1 compares the metasurface-based antenna to state-of-the-art methods in size, bandwidth, gain, and printed layers. The proposed antenna has a compact size, single printed layer, low profile, and peak gain by using fewer unit cells than previous designs. Multiple printed layers complicate antenna design in [18], [20]. Radial-phase gradient metalens has a higher gain but a larger antenna profile and complex design due to different unit cell structures [19]. MIMO antennas with circular split-ring resonators [21], slotted patch antennas, and metasurfaces [22], [23] improve gain but have a higher antenna profile and more unit cells. End-fire dipole array uses similar substrate for circular patches and crossslot-based metasurface with different height provides good gain at the cost of fabrication complexity [28]. The proposed design uses a similar substrate material with the same thickness for metasurface and primary patch antenna and is compact. However, the AR performance is little bit deteriorates due to loading of metasurface, and an additional strategies can be incorporated in the metasurface design to increase the bandwidth.

Table 1. Comparison of existing literature in relation to the proposed work

Ref	Antenna Size (λ_0^3)	Array size	*IBW(%)	*ARBW (%)	Gain (dBiC)	MTS layers	Polarization
[18]	2.6 × 2.6 × 0.4	7×7	15.5	-	17.78	2	LP
[19]	4.6 × 4.6 × 1.8	10×10	5.2	-	12.4	1	LP
[20]	2.6 × 2.6 × 0.4	-	12.5	-	7.4	3	LP
[21]	2.5×3.6×0.4	9×6	7.84	-	10.2	1	LP
[22]	1.2×1.3×0.6	8×8	17	-	12.7	1	LP
[23]	2.8×4.1×0.8	9×6	13.8	-	12.9	1	LP
[28]	2.9×2.9×0.4	4×4	21.5	15.5	11	1	CP
[proposed]	1.1 × 1.1 × 0.2	3×3	6.14	1.39	11.5	1	CP

4. CONCLUSION

For millimeter-wave applications, the proposed design demonstrates the effectiveness of a metasurface-based compact high-gain, circularly polarized antenna. The experimentally measured impedance bandwidth of 28.23–30.01 GHz is achieved and maintained with less than 3 dB axial ratio over a bandwidth of 28.45–28.88 GHz. The designed antenna achieves a peak gain of 11.5 dBic with a cross-polarization value of -20 dB with respect to co-polarization, this guarantees a consistent radiation pattern throughout the entire operating band. Radiation efficiency of more than 80% is attained, rendering the proposed antenna appropriate for 5G millimeter-wave networks due to its compact size of $1.34\lambda_0^2$, cost-effectiveness and compatibility with handheld wireless devices. Since it offers an optimal solution for these networks, future work will focus on improving the operational axial ratio bandwidth and exploring additional applications in emerging wireless communication technologies.

REFERENCES

[1]   J. Thompson *et al.*, "5G wireless communication systems: prospects and challenges [Guest Editorial]," *IEEE Communications Magazine*, vol. 52, no. 2, pp. 62–64, Feb. 2014, doi: 10.1109/mcom.2014.6736744.

[2]   C.-X. Wang *et al.*, "Cellular architecture and key technologies for 5G wireless communication networks," *IEEE Communications Magazine*, vol. 52, no. 2, pp. 122–130, Feb. 2014, doi: 10.1109/mcom.2014.6736752.

[3]   R. Vannithamby and S. Talwar, *Towards 5G: applications, requirements and candidate technologies*. Wiley Telecom, 2017.

[4]   "Spectrum for 4G and 5G," 2019. .

[5]   B. T. Jijo *et al.*, "A comprehensive survey of 5G mm-wave technology design challenges," *Asian Journal of Research in Computer Science*, pp. 1–20, Apr. 2021, doi: 10.9734/ajrcos/2021/v8i130190.

[6]   W. Hong *et al.*, "mmWave 5G NR cellular handset prototype featuring optically invisible beamforming antenna-on-display," *IEEE Communications Magazine*, vol. 58, no. 8, pp. 54–60, Aug. 2020, doi: 10.1109/mcom.001.2000115.

[7]   P. Ramanujam, C. Arumugam, R. Venkatesan, and M. Ponnusamy, "Design of compact patch antenna with enhanced gain and bandwidth for 5G mm-wave applications," *IET Microwaves, Antennas & Propagation*, vol. 14, no. 12, pp. 1455–1461, Jul. 2020, doi: 10.1049/iet-map.2019.0891.

[8]   K. M. Mak, H. W. Lai, K. M. Luk, and C. H. Chan, "Circularly polarized patch antenna for future 5G mobile phones," *IEEE Access*, vol. 2, pp. 1521–1529, 2014, doi: 10.1109/access.2014.2382111.

[9]   G. Kim and S. Kim, "Design and analysis of dual polarized broadband microstrip patch antenna for 5G mmWave antenna module on FR4 substrate," *IEEE Access*, vol. 9, pp. 64306–64316, 2021, doi: 10.1109/access.2021.3075495.

[10]   A. Dadgarpour, M. Sharifi Sorkherizi, and A. A. Kishk, "High-efficient circularly polarized magnetoelectric dipole antenna for 5G applications using dual-polarized split-ring resonator lens," *IEEE Transactions on Antennas and Propagation*, vol. 65, no. 8, pp. 4263–4267, Aug. 2017, doi: 10.1109/tap.2017.2708091.

[11]   A. Y. I. Ashyap *et al.*, "An overview of electromagnetic band-gap integrated wearable antennas," *IEEE Access*, vol. 8, pp. 7641–7658, 2020, doi: 10.1109/access.2020.2963997.

[12]   H. H. Tran, C. D. Bui, N. Nguyen-Trong, and T. K. Nguyen, "A wideband non-uniform metasurface-based circularly polarized reconfigurable antenna," *IEEE Access*, vol. 9, pp. 42325–42332, 2021, doi: 10.1109/access.2021.3066182.

[13]   P. K. T. Rajanna, K. Rudramuni, and K. Kandasamy, "A high-gain circularly polarized antenna using zero-index metamaterial," *IEEE Antennas and Wireless Propagation Letters*, vol. 18, no. 6, pp. 1129–1133, Jun. 2019, doi: 10.1109/lawp.2019.2910805.

[14]   M. Alibakhshikenari *et al.*, "A comprehensive survey on various decoupling mechanisms with focus on metamaterial and metasurface principles applicable to SAR and MIMO antenna systems," *IEEE Access*, vol. 8, pp. 192965–193004, 2020, doi: 10.1109/access.2020.3032826.

[15]   M. J. Jeong, N. Hussain, J. W. Park, S. G. Park, S. Y. Rhee, and N. Kim, "Millimeter-wave microstrip patch antenna using vertically coupled split ring metaplate for gain enhancement," *Microwave and Optical Technology Letters*, vol. 61, no. 10, pp. 2360–2365, Jun. 2019, doi: 10.1002/mop.31908.

[16]   P. K. T. Rajanna, K. Rudramuni, and K. Kandasamy, "A wideband circularly polarized slot antenna backed by a frequency selective surface," *Journal of Electromagnetic Engineering and Science*, vol. 19, no. 3, pp. 166–171, Jul. 2019, doi: 10.26866/jees.2019.19.3.166.

[17]   S. X. Ta, N. Nguyen-Trong, V. C. Nguyen, K. K. Nguyen, and C. Dao-Ngoc, "Broadband dual-polarized antenna using metasurface for full-duplex applications," *IEEE Antennas and Wireless Propagation Letters*, vol. 20, no. 2, pp. 254–258, Feb. 2021, doi: 10.1109/lawp.2020.3047231.

[18]   M. Asaadi, I. Afifi, and A.-R. Sebak, "High gain and wideband high dense dielectric patch antenna using FSS superstrate for millimeter-wave applications," *IEEE Access*, vol. 6, pp. 38243–38250, 2018, doi: 10.1109/access.2018.2854225.

[19]   P. Das and A. K. Singh, "Gain enhancement of millimeter wave antenna by ultra-thin radial phase gradient metasurface for 5G applications," *IETE Journal of Research*, vol. 70, no. 3, pp. 2400–2408, Mar. 2023, doi: 10.1080/03772063.2023.2191998.

[20]   H. Jiang, L.-M. Si, W. Hu, and X. Lv, "A symmetrical dual-beam bowtie antenna with gain enhancement using metamaterial for 5G MIMO applications," *IEEE Photonics Journal*, vol. 11, no. 1, pp. 1–9, Feb. 2019, doi: 10.1109/jphot.2019.2891003.

[21]   S. Tariq, S. I. Naqvi, N. Hussain, and Y. Amin, "A metasurface-Based MIMO antenna for 5G millimeter-wave applications," *IEEE Access*, vol. 9, pp. 51805–51817, 2021, doi: 10.1109/access.2021.3069185.

[22]   C. M. Saleh, E. Almajali, A. Jarndal, J. Yousaf, S. S. Alja'Afreh, and R. E. Amaya, "Wideband 5G antenna gain enhancement using a compact single-layer millimeter wave metamaterial lens," *IEEE Access*, vol. 11, pp. 14928–14942, 2023, doi: 10.1109/access.2023.3244401.

[23]   N. A. Rao, L. B. Konkyana, V. L. Raju, M. S. R. Naidu, and C. R. Babu, "A broadband meta surface based MIMO antenna with high gain and isolation For 5G millimeter wave applications," *International Journal of Communication Networks and Information Security (IJCNIS)*, vol. 14, no. 1s, pp. 54–66, Jan. 2023, doi: 10.17762/ijcnis.v14i1s.5592.

[24]   N. Hussain, M.-J. Jeong, J. Park, and N. Kim, "A broadband circularly polarized fabry-perot resonant antenna using a single-layered PRS for 5G MIMO applications," *IEEE Access*, vol. 7, pp. 42897–42907, 2019, doi: 10.1109/access.2019.2908441.

[25]   N. Nguyen-Trong, H. H. Tran, T. K. Nguyen, and A. M. Abbosh, "A compact wideband circular polarized fabry-perot antenna using resonance structure of thin dielectric slabs," *IEEE Access*, vol. 6, 2018, doi: 10.1109/access.2018.2872571.

[26]   N. Hussain, M.-J. Jeong, A. Abbas, T.-J. Kim, and N. Kim, "A metasurface-based low-profile wideband circularly polarized patch antenna for 5G millimeter-wave systems," *IEEE Access*, vol. 8, pp. 22127–22135, 2020, doi: 10.1109/access.2020.2969964.

[27]   N. Hussain, M.-J. Jeong, A. Abbas, and N. Kim, "Metasurface-based single-layer wideband circularly polarized MIMO antenna for 5G millimeter-wave systems," *IEEE Access*, vol. 8, pp. 130293–130304, 2020, doi: 10.1109/access.2020.3009380.

[28]   C. H. S. Nkimbeng, H. Wang, G. Byun, Y. B. Park, and I. Park, "Non-uniform metasurface-integrated circularly polarized end-fire dipole array antenna," *Journal of Electromagnetic Engineering and Science*, vol. 23, no. 2, pp. 109–121, Mar. 2023, doi: 10.26866/jees.2023.2.r.150.

[29]   X. Zhang, S. Tong, J. Wang, and X. Feng, "Wideband circularly polarized millimeter-wave metasurface antenna array feed by SIW," *International Journal of RF and Microwave Computer-Aided Engineering*, vol. 32, no. 10, Jul. 2022, doi: 10.1002/mmce.23322.

[30]   R. Przesmycki, M. Bugaj, and L. Nowosielski, "Broadband microstrip antenna for 5G wireless systems operating at 28 GHz," *Electronics*, vol. 10, no. 1, p. 1, Dec. 2020, doi: 10.3390/electronics10010001.

[31]   C. A. Balanis, *Antenna theory: analysis and design*. Fourth Edition. John Wiley Publications, 2016.

[32]   I. J. Bahl and P. Bhartia, *Microstrip antennas*. Artech House, 1980.

[33]   D. M. Pozar, "Microwave engineering education: From field theory to circuit theory," in *2012 IEEE/MTT-S International Microwave Symposium Digest*, Jun. 2012, vol. 8, pp. 1–3, doi: 10.1109/mwsym.2012.6259373.

[34] J. R. James and P. S. Hall, *Handbook of Microstrip Antennas*. London, U.K.: Peter Peregrinus, 1989.

[35] K. Agarwal, Nasimuddin, and A. Alphones, "Wideband circularly polarized amc reflector backed aperture antenna," *IEEE Transactions on Antennas and Propagation*, vol. 61, no. 3, pp. 1456–1461, Mar. 2013, doi: 10.1109/tap.2012.2227446.

[36] X. Li, J. Yang, Y. Feng, M. Yang, and M. Huang, "Compact and broadband antenna based on a step-shaped metasurface," *Optics Express*, vol. 25, no. 16, p. 19023, Jul. 2017, doi: 10.1364/oe.25.019023.

[37] F. Costa, O. Luukkonen, C. R. Simovski, A. Monorchio, S. A. Tretyakov, and P. M. de Maagt, "TE surface wave resonances on high-impedance surface based antennas: analysis and modeling," *IEEE Transactions on Antennas and Propagation*, vol. 59, no. 10, pp. 3588–3596, Oct. 2011, doi: 10.1109/tap.2011.2163750.

[38] D. Ferreira, R. F. S. Caldeirinha, I. Cuinas, and T. R. Fernandes, "Square loop and slot frequency selective surfaces study for equivalent circuit model optimization," *IEEE Transactions on Antennas and Propagation*, vol. 63, no. 9, pp. 3947–3955, Sep. 2015, doi: 10.1109/tap.2015.2444420.

[39] G. V Trentini, "Partially reflecting sheet arrays," *IRE Transactions on Antennas and Propagation*, vol. 4, no. 4, pp. 666–671, Oct. 1956, doi: 10.1109/tap.1956.1144455.

BIOGRAPHIES OF AUTHORS

Praveen Haandi Lakshman received his undergraduate degree in the Department of Electronics and Communication Engineering from Visvesvaraya Technological University, Karnataka, India, in 2009 and Postgraduate degree in Digital Electronics from Sri Siddhartha University, Tumakuru, Karnataka, India in 2012. He is currently working as an Assistant Professor in the Department of Electronics and Communication Engineering, Shri Dharmasthala Manjunatheshwara Institute of Technology, Ujire, Karnataka and pursuing his Ph.D. degree under Visvesvaraya Technological University (VTU), Karnataka, India. His field of research includes Metamaterial based antennas, Characteristic mode Analysis, RF circuits, Microwave antennas, and Microstrip antennas. He can be contacted at email: praveee79@gmail.com.

Yerriswamy Thatti received his BE in Electronics and Communication Engineering from Gulbarga university, India in 2000, MTech degree in Network and Internet Engineering and PhD in Antenna array Signal Processing in the year 2012 from Visvesvaraya Technological University. He is currently working as Professor at KLE Institute of Technology, India. His area of research includes antenna arrays, antenna array signal processing, and data-driven signal processing. He can be contacted at email: swamy1976ty@gmail.com.

Puneeth Kumar Tharehalli Rajanna received the B.E. degree in Telecommunication engineering, M.Tech. degree in Digital Communication engineering from Visveswaraya Technological University (VTU), Belgaum, Karnataka, India, in 2009 and 2013, respectively, and Ph.D. degree in Electronics and Communication Engineering (Antennas and RF circuits) from the National Institute of Technology Karnataka, Surathkal, India, in 2020. He is currently working as an Assistant Professor at the Department of Electronics and Telecommunication Engineering, Siddaganga Institute of Technology, Tumkur, India, affiliated to VTU. His field of research includes metamaterial-based antennas, characteristic mode analysis, leaky wave antennas, MMICs, RF circuits, microwave antennas, and microstrip antennas. He can be contacted at email: punithkumartr@sit.ac.in.

Shambulinga Mudukavvanavar received the B.E. degree in Electronics and communication engineering, M.Tech. degree in Digital Communication engineering and Ph.D. in Image Processing from Visveswaraya Technological University (VTU), Belgaum, Karnataka, India, in 2011, 2013 and 2022 respectively. He is currently working as an Assistant Professor at the Department of Electronics and Telecommunication Engineering, RV college of Engineering, Bengaluru, India, affiliated to VTU. His field of research includes image processing, computer vision, RF and microwave circuits and antennas. He can be contacted at email: shambulinga.m@rvce.edu.in.